



Aerothermal Measurements from the ExoMars Schiaparelli Capsule Entry

A. Gülhan,* T. Thiele,† F. Siebe,† R. Kronen,† and T. Schleutker†
DLR, German Aerospace Center, 51147 Cologne, Germany

DOI: 10.2514/1.A34228

The instrumentation package COMARS+ was developed to measure aerothermal parameters on the back cover of the ExoMars Schiaparelli lander during Martian entry. The aerothermal sensors called Combined Aerothermal and Radiometer Sensor (COMARS) combine four discrete sensors, measuring static pressure, total heat flux, temperature, and radiative heat flux. After passing all acceptance tests, the Schiaparelli capsule was launched on top of the Proton launcher on March 14, 2016. All COMARS+ sensors operated nominally during the complete entry phase. But the complete data package is not available due to an anomaly that led to the failure of Schiaparelli shortly before landing. Nevertheless, a subset of the COMARS+ flight data was transmitted real-time during the entry and was received by the ExoMars 2016 orbiter, with the exception of the plasma blackout phase. The radiative heat flux on the back cover close to the vehicle shoulder was measured successfully for the first time on a Mars entry vehicle. The measured maximum radiative contribution was 61% of the total heat flux at the first measurement point after the blackout phase and 33% for the next measured trajectory point 10 s later. These measurements confirm recent findings that radiative heating can be a significant portion of total heating on the back cover during Mars entry. The maximum back cover total heat flux rate was measured at approximately 9% of the calculated stagnation point heat flux on the front cover. All measured heat fluxes on the back cover were below the levels that were used to design the thermal protection system.

Nomenclature

c_p	=	pressure coefficient
h	=	enthalpy, J/kg
k	=	constant (Sutton–Graves formula), $\sqrt{\text{kg/m}}$
M	=	Mach number
p	=	pressure, Pa
q	=	dynamic pressure, Pa
\dot{q}	=	heat flux, W/m^2
\dot{q}_s	=	stagnation point heat flux, W/m^2
Re	=	Reynolds number
R_n	=	nose radius (equivalent nose radius), m
St	=	Stanton number
T	=	temperature, K
t	=	time, s
u	=	velocity, m/s
x, y, z	=	coordinates, m
ρ	=	density, kg/m^3

Subscripts

meas	=	measured
w	=	wall condition
∞	=	atmospheric (inflow) parameter
0	=	total condition

I. Introduction

THE first mission of the ExoMars program, which arrived at Mars in October 2016, consisted of a trace gas orbiter (TGO)

Received 19 February 2018; revision received 4 May 2018; accepted for publication 16 May 2018; published online Open Access 26 June 2018. Copyright © 2018 by DLR, German Aerospace Center. Published by the American Institute of Aeronautics and Astronautics, Inc., with permission. All requests for copying and permission to reprint should be submitted to CCC at www.copyright.com; employ the ISSN 0022-4650 (print) or 1533-6794 (online) to initiate your request. See also AIAA Rights and Permissions www.aiaa.org/randp.

*Head of the Supersonic and Hypersonic Technologies Department, Institute of Aerodynamics and Flow Technology, Principle Investigator of the COMARS+ Instrumentation Package.

†Research Scientist at the Supersonic and Hypersonic Technologies Department, Institute of Aerodynamics and Flow Technology.

plus an entry, descent, and landing demonstrator module (EDM) named “Schiaparelli.” The orbiter and Schiaparelli were launched on March 14, 2016, on a Proton rocket. The main scientific objectives of this mission were to search for evidence of methane and other trace atmospheric gases that could be signatures of active biological or geological processes and to test key technologies in preparation for ESA’s contribution to subsequent missions to Mars. The demonstration of a successful entry, descent, and landing (EDL) and the collection of data during this mission phase are considered to be extremely important contributions to risk reduction for future Mars missions. These data could be used for an optimization of the thermal protection system (TPS), because the design of the back cover heat shield was carried out with relatively high safety margins. This is because the prediction of aerothermal loads on the back cover, using existing experimental and numerical tools, still has large uncertainties.

The design of the Schiaparelli heat shield was carried out using an aerothermodynamic database for the ExoMars entry demonstrator module (EDM), which includes convective and radiative heat flux calculations. The convective heat fluxes were determined using computational fluid dynamics (CFD) tools validated against dedicated wind tunnel tests. Conservative assumptions were employed for the catalysis of recombination reactions at the surface and augmentation of heat fluxes by surface roughness. The calculated radiative heat fluxes also include the effects of infra-red radiation from CO_2 molecules. Especially on the vehicle back cover the contribution of radiative heat flux to the total heat flux is significant. Aerothermodynamic pre-flight CFD calculations including the comparison of different numerical codes are given in [1–3].

The United States has instrumented some of its successful planetary entry capsules, including those that landed on Mars. However, the volume of data is much less than what is needed to address aerothermal environments margins, especially on the capsule aftbody. The first successful mission to Mars, which also included TPS instrumentation, was Viking Lander 1 in 1976. The preflight prediction of the Viking afterbody heating, including a safety factor of 1.5, estimated a maximum heat flux value of 3% of the nose laminar heating [4,5]. But postflight analysis of the temperature data showed that a value of 4.2% was reached. It has to be mentioned that Viking Lander 1 was only instrumented with thin-film gauges at two locations on the back cover, which were spot-welded to aluminum and fiberglass. A heat flux rate of 9.7 kW/m^2 was derived from the thermocouple data on the aluminum structure at the time of sensor

failure. On the fiberglass cover the sensor worked during the complete entry, and a peak heating value of 6.6 kW/m^2 was determined [5]. A very interesting finding of this study is the delayed peak heating on the back cover compared with the front cover peak heating.

Very high heat fluxes occurred during the Galileo probe entry into the Jovian atmosphere in 1995. The Galileo probe entered the atmosphere with a relative velocity of 47.4 km/s and was exposed to heat fluxes up to 170 MW/m^2 . The capsule was instrumented with analog resistance ablation detectors (ARAD) and four thermometers to measure the TPS recession [6]. Two thermometers were placed on the back cover and used to predict the rear surface recession based on the front cover recession measured by the ARAD sensors. Because of uncertainties in the front cover data, it was difficult to assess the afterbody heating.

Another successful Mars landing was performed by Mars Pathfinder in 1997, which included the first Mars rover. The aftbody frustum of Pathfinder vehicle was coated with a spray-on version of the super lightweight ablator (SLA), named "SLA-561S." The honeycomb-packed version (SLA-561V) was used on Pathfinder's forebody. The backshell interface plate and the rear portion of the frustum were covered with silicone-impregnated reusable ceramic ablator (SIRCA) tiles and had no surface-mounted instrumentation. But the aeroshell did contain nine thermocouples at various depths in the TPS material and three platinum resistance thermometers [7]. Unfortunately some thermocouples failed to provide useable data. For one near-surface thermocouple on the backshell the peak temperature could be matched to the predicted turbulent corner heating scaled by 0.026, but with an incorrect shape of the thermocouple response.

In general the TPS design of an entry capsule is carried out using numerical tools and ground experiments. The aerothermal design and sizing of the TPS of Mars capsules are carried out using CFD codes and ablative material response tools, which are calibrated through ground experiments. The reliability of these design tools is essential for the design margin of spacecraft structures. Because the physical models in the numerical tools can only be validated partially, the design requires high safety margins, that is, more mass in the vehicle design. Assumptions such as supercatalytic wall, fully turbulent flow environment, and strong roughness-induced heat flux augmentation lead to more than 40% extra forebody TPS thickness [8,9], which in turn has a significant impact on the overall mass budget.

To improve data return value for Mars entries, the heat shield of the Mars science laboratory (MSL), which successfully landed in 2012, was instrumented with several sensors related to aerodynamics, aerothermal heating, and performance of the TPS [10,11]. The installed MSL sensor package Mars science laboratory entry, descent, and landing instrumentation (MEDLI) collected pressure, temperature, and recession data on the front TPS [12]. The pressures were measured by the Mars entry atmospheric data system (MEADS), and in-depth temperatures were measured by the MEDLI integrated sensor plugs (MISP). MEADS and MISP sensors were distributed over the MSL front cover TPS at seven independent locations each. The MEADS part contains a flush airdata sensing (FADS) system that collects surface pressures during flight. The pressure ports are arranged in such a way that aerodynamic parameters (e.g., angle of attack) can be computed from measured pressure values. In addition the measured pressure data allow verification of the trajectory reconstruction algorithm for MSL [13,14]. The MISP is a cylindrical PICA plug with four type-K (chromel-alumel) thermocouples in different depths. In addition to the thermocouples a sensor called hollow aerothermal ablation and temperature (HEAT) is also installed in the plug to track the ablation process. During Mars entry the MISP temperature data showed the occurrence of boundary-layer transition on the leeward side of the MSL forebody. The data also indicate that the thermal protection system recession was below predicted values.

The ExoMars program sought to collect data from Schiaparelli similar to what MEDLI measured. To determine the overall performance and for trajectory reconstruction of Schiaparelli, the front cover was instrumented with four pressure sensors and seven thermal plugs. Each thermal plug contained three thermocouples plus

one thermistor behind the plug [15–17]. Previous Mars missions that included instrumentation were mainly focused on the front cover TPS due to the higher heat loads. An overview of aftbody aeroheating flight data for planetary entry probes is given in the paper of Wright et al. [18]. This paper recommends that for the reduction of mass and risk future planetary entry vehicles should include TPS instrumentation. The aftshell is suggested as the safest place to incorporate instrumentation because of the low heating rates.

In contrast to the MSL instrumentation, the Schiaparelli capsule also included several sensors on the back cover. In this region the Reynolds number of the flow is low, which results in comparatively low convective heat fluxes. But the radiative heat flux, mainly resulting from excitation of carbon dioxide molecules behind the strong bow shock, can exceed the convective heat flux. The simulation of aftbody radiation in a Mars environment using ground test facilities is difficult due to numerous challenges. However, preflight analysis suggested that the radiative component of the heat flux would not be negligible on the capsule back cover due to CO_2 infrared emissions [3,19]. To close this gap and measure aerothermal flight data on the Schiaparelli back cover, the supersonic and hypersonic technology department of the German aerospace center (DLR) in Cologne developed the combined aerothermal sensor package COMARS+, based on experience gathered during the flight instrumentation for the flight experiments SHEFEX-I and SHEFEX-II [20,21]. The COMARS+ instrumentation package consists of three combined aerothermal sensors (called COMARS), one broadband radiometer sensor, and an electronic box [22]. The aerothermal sensors combine four discrete sensors to measure static pressure, total heat flux, temperature, and radiative heat flux at two specific spectral bands. The infrared radiation in a broadband spectral range is measured by the separate broadband radiometer sensor. The electrical interface between sensors and Schiaparelli data handling system is provided by the payload electronic box.

Although the landing of Schiaparelli failed, part of the flight data during the entry phase was transmitted to the orbiter at a low sampling rate from the atmospheric entry point until parachute deployment with the exception of the plasma blackout phase. All COMARS+ sensors successfully measured surface pressure and total and radiative heat flux at the transmitted trajectory points. Especially important is the high contribution of radiative heat flux, which was measured for the first time on a Mars entry vehicle, to the total heat flux on the back cover.

This paper describes the main properties of the COMARS+ payload, mechanical and thermal design details, some results of aerothermal tests performed in the arc-heated facility L2K at DLR Cologne, and a detailed discussion of the measured flight data.

II. Requirements and Design Approach

The COMARS+ instrumentation package was proposed for the Schiaparelli capsule back cover to gain reliable flight data and to assess the design margins for the Schiaparelli TPS. The COMARS+ payload had to satisfy a large matrix of requirements:

- 1) COMARS+ may not cause any risk to the success of the mission.
- 2) The total mass of the payload shall be less than 2 kg, including maturity margins.
- 3) The dimensions shall be as small as possible considering the required fixations and available envelope.
- 4) The average power consumption shall stay below 7 W at an operative voltage between 22 and 36 V.
- 5) Qualification tests, acceptance tests, and documentation must be performed according to the European cooperation for space standardization (ECSS).
- 6) The heat flux sensor shall be able to measure total heat fluxes up to 150 kW/m^2 .
- 7) The radiometer sensor shall be able to measure radiative heat fluxes up to 100 kW/m^2 .
- 8) The pressure sensor shall be able to measure surface pressures up to 300 Pa.

Table 1 COMARS+ payload overview

Unit name	Description
Multiplexing signal conditioner (MSC)	Electronic box
COMARS1 (COM 1)	Combined static pressure, total heat-flux, Temperature, and two CNES spectral radiometer sensors (ICOTOM)
COMARS2 (COM 2)	
COMARS3 (COM 3)	
Radiometer (RAD)	Broadband radiometer
Payload harness	Harness connecting the sensors to the electronic box

These requirements forced DLR to significantly modify the SHEFEX sensor design and miniaturize sensor heads and electronics to the Schiaparelli mission [21,22]. Several thermal and mechanical analyses were performed for verification of the chosen design. To verify the preliminary design and general functionality of the components, two sets of engineering models were manufactured. A set of qualification models (one COMARS sensor, one broadband radiometer sensor, and one electronic box) was manufactured and subjected to mechanical, thermal/vacuum, shock, radiation hardness, electromagnetic compatibility, and aerothermal tests at conditions defined by ESA and Thales Alenia Space Italy (TAS-I). In addition to these tests, the cleaning procedure for planetary protection requirements was tested on the qualification models to demonstrate that the number of spores could be reduced to the necessary level. One set of flight models was manufactured (three COMARS sensors, one broadband radiometer sensor, and one electronic box) for integration into the Schiaparelli capsule. A spare part for each individual component was made in addition.

The ExoMars EDM mission (2016) was classified as Planetary Protection Category IVa, being a landed system without life-detection experiments nor accessing a “special region” of Mars. The bioburden constraints for COMARS+ at delivery were defined as:

1) Bioburden ≤ 1000 bacterial spores on COMARS+ exposed internal and external surfaces.

2) Average bioburden density ≤ 300 bacterial spores/m² on the COMARS+ exposed internal and external surfaces.

3) All COMARS+ harnesses, including hardware isolated by equivalent high-efficiency particulate air (HEPA) filters (H14 classification), shall be processed with dry heat microbial reduction (DHMR) using six D-values for encapsulated bioburden, to reduce the number of encapsulated spores below the threshold for COMARS+. The D-value at 125°C DHMR temperature for encapsulated bioburden amounts to 5 h according to planetary protection requirements.

4) The encapsulated spores for COMARS+ payload shall number less than 13,200.

All flight and spare components were assembled in a clean room environment and subjected to a bioburden reduction process to satisfy these requirements.

III. Payload Layout

The combined aerothermal sensors designed for the SHEFEX-II Earth flight experiment were changed for Schiaparelli to account for different TPS thickness, fixation method, available space, and temperature environment as described in Ref. [23]. The interface was manufactured from titanium instead of stainless steel to keep the mass as low as possible for Schiaparelli. Because of the very low pressure and limited space a different pressure sensor was used. A good compromise was found in a Pirani-type pressure sensor, which is small and able to measure pressures down to a few Pascal. The cabling of the commercial heat flux microsensor (HFM) of Vatel used for SHEFEX-II was adapted to fit into the new sensor interface. Furthermore the sensor interface was extended to incorporate two radiometers that measure the radiative heat flux at two specific spectral bands. These radiometers called ICOTOM were contributed by the French space agency CNES [24,25] and were specifically designed for the ExoMars Schiaparelli lander. The infrared radiation in a broadband spectral range was measured by a separate broadband radiometer sensor that was developed for the ExoMars mission. The radiometer consists of a thermopile integrated into a titanium sensor interface. The outer dimensions and fixation points of the broadband radiometer interface are identical to the COMARS sensor to minimize the number of different mechanical interfaces at the back cover. Table 1 presents an overview of the different parts of the COMARS+ instrumentation package.

Overall 23 sensor and 8 housekeeping signals need to be amplified to a specified input voltage range and multiplexed to three analog acquisition channels of the EDM data handling system. This requirement is accomplished using an electronic box that is also part of the payload. In addition to amplification and multiplexing, signal conditioning is also integrated in the electronic layout. The digitization of the sensor signals is done by the capsule on-board data handling system and was not part of the COMARS+ payload. The analog sensor signals were digitized with a 12-bit resolution and a sampling frequency of 10 Hz.

The locations of the three COMARS sensors and the broadband radiometer on the Schiaparelli back cover are shown in Fig. 1.

The COMARS sensors and the broadband radiometer are fixed to the ExoMars back cover structure using honeycomb inserts to which the sensors are attached with four M4 screws each. Figures 2 and 3 show exterior and interior views of the COMARS sensor with denomination of the different parts.

The Multiplexing Signal Conditioner (MSC, COMARS+ electronic box) consists of one multiplexing board and one power board mounted on top of each other in an aluminium housing. The layout of the MSC is shown in Fig. 4 and consists of one multiplexing board and one power board in an aluminium housing. The multiplexing board contains amplifiers, filters, and the multiplexing circuit for the sensor signals. The power board generates the necessary voltage levels from the unregulated bus of the EDM using a DC/DC converter. The sensor signal multiplexing is controlled via clock and synchronization signals from the EDM data handling

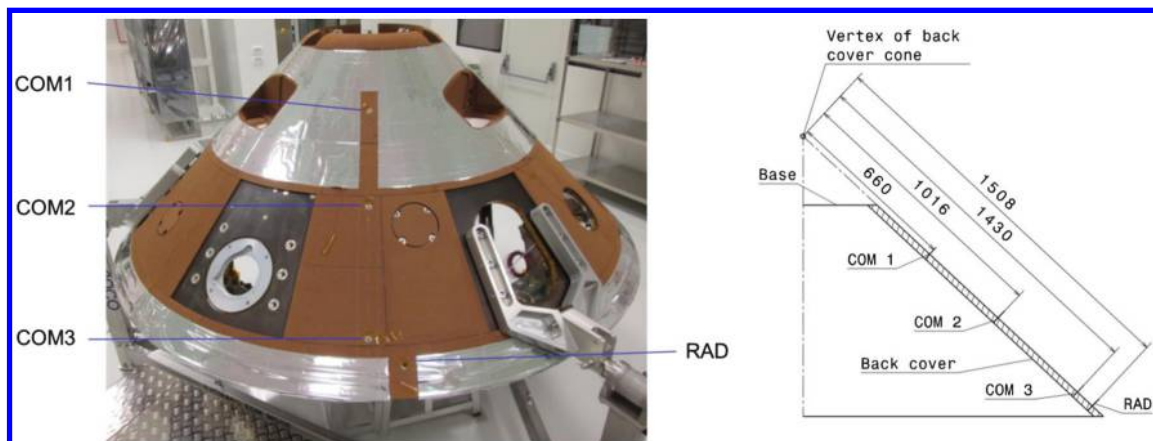


Fig. 1 Position of COMARS+ sensors on the back cover of Schiaparelli.

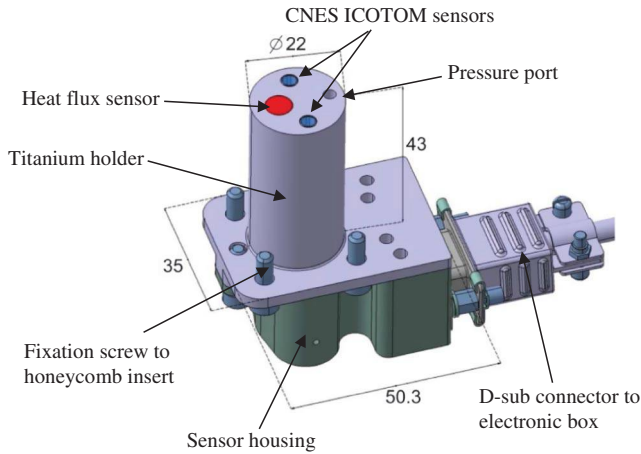


Fig. 2 COMARS sensor assembly top view with dimensions (mm).

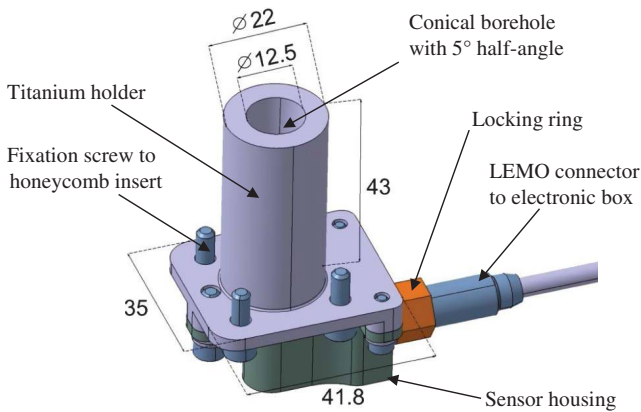


Fig. 3 Broadband radiometer top view with dimensions (mm).

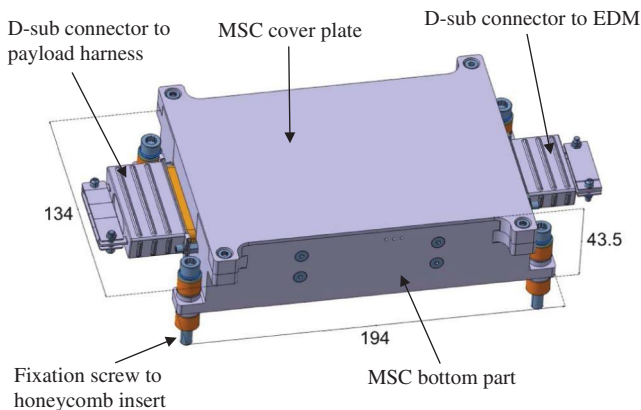


Fig. 4 Electronic box top view with dimensions (mm).

system. The electronic box was also attached to the inner surface of the back cover using four honeycomb inserts. The box was located beside COMARS sensor 2 to minimize the harness length between electronic box and sensors. More information about sensors and electronic box is given in Ref. [23].

IV. Structural and Thermal Design

A. Structural Analysis

Several structural analyses were performed to verify the structural integrity of the COMARS+ components during the launch phase. The electronic box is the heaviest part of the payload with a weight of

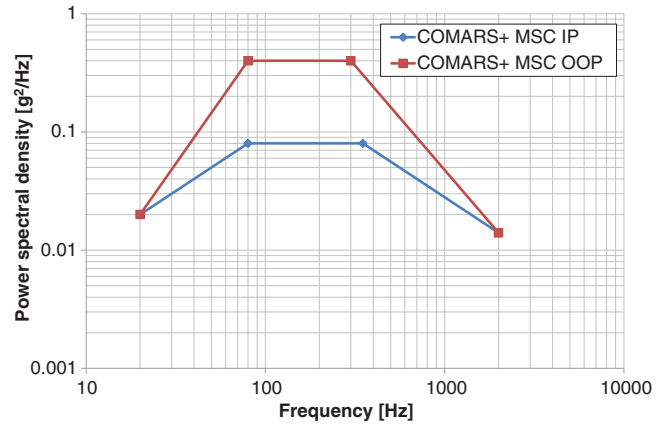


Fig. 5 Random vibration loads of COMARS+ electronic box.

920 g (with margins) and is therefore exposed to the highest mechanical stresses. Some results from the numerical analysis of the electronic box are shown below.

A simple worst-case analysis of the mechanical loads acting on the electronic box during launch and ascent was conducted using the random vibration loads at qualification level (Fig. 5). The necessary accelerations for the structural analysis were derived from the random vibration loads using the Miles equation [26]. The Miles equation is a simplified method of calculating the response of a system to a random vibration input, assuming that the fundamental mode in each orthogonal direction will provide the primary system response (the system is assumed to have only one degree of freedom). The equation calculates the corresponding root mean square acceleration (G_{rms}) using a power spectral density (PSD), the fundamental frequency of the system, and an amplification factor. Multiplying the G_{rms} value by three (3σ load) gives the equivalent static load, which is referred to as the random vibration load factor (RVLf). The amplification factor describes the amplification of the input acceleration at resonance and is, for example, determined via a sine sweep test. If no test data is available, an amplification factor of 10 should be used for most components. The fundamental frequency of the electronic box was not taken into account for the worst-case analysis, but the RVLf was calculated for the complete random vibration frequency range between 20 and 2000 Hz, and the maximum calculated acceleration was used for the mechanical analysis. The amplification factor was set to 16, which was the maximum value measured on the electronic box bottom during the sine sweep test in the frame of the qualification test campaign. This amplification factor was used for in-plane and out-of-plane direction. It has to be noted that the static loads evaluated using the described approach represent very conservative values.

In Fig. 6 the equivalent static load curve is plotted for the complete frequency range of 20–2000 Hz. The maximum values of 233 g

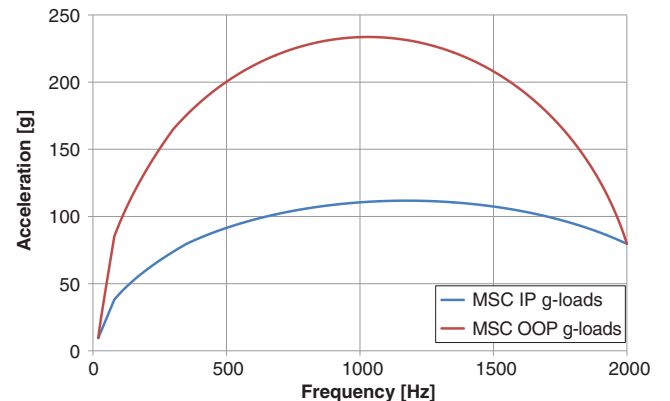


Fig. 6 COMARS+ electronic box static load curve derived from random loads.

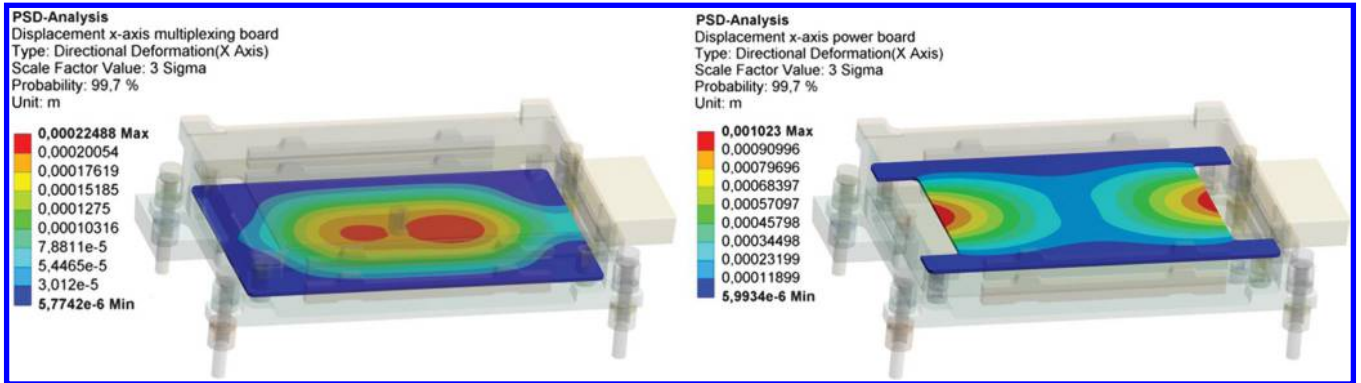


Fig. 7 PSD analysis for electronic box: deflection of multiplexing board (left) and power board (right).

(out-of-plane, OOP) and 111 g (in-plane, IP) were used for the structural analysis. The out-of-plane direction is thereby defined as the direction perpendicular to the electronic box mounting plane and the in-plane directions are parallel to the edges of the MSC top plate.

Some simplifications were made for the finite element model (FEM) with respect to detailed interfaces, screws, and printed circuit boards (PCB), but the overall mass of the box was kept constant. The resulting von Mises equivalent stress value of 106 MPa for the electronic box occurred at the mounting feet and was well below the yield strength of the aluminium material (380 MPa). The calculated stresses for the attachment components (screws, spacers, thermal washers) were also below the corresponding material stress limits. In addition to the structural analyses, modal analyses were performed for the sensors and electronic box to determine the first fundamental frequencies. The results showed that all fundamental frequencies are above the limit frequency of 140 Hz specified in the ExoMars mechanical interface requirements.

A power spectral density analysis was performed to determine the maximum deflection of the PCBs inside the electronic box, using the random vibration loads shown in Fig. 5. Figure 7 shows the deflection of the multiplexing and power boards perpendicular to the board plane. The results were computed for a 3σ probability (standard deviation) so that the board deflections are below the shown values with a probability of 99.7%. The maximum deflection of the multiplexing board occurs near the center. A fixation screw is placed in the center of the PCB, leading to a deflection maximum of 0.2 mm, which is considered acceptable for the multiplexing board. The maximum deflection of the power board is larger at 1.0 mm on the short sides because the board is not fixed to the electronic box structure along these sides. The components on the power board (DC/DC converter, voltage filter) are placed near the center of the PCB, where the deflections are lower, and are additionally fixed with epoxy adhesive, and so the larger deflection of the power board is not an issue.

B. Thermal Analysis

Transient analyses were performed to verify the thermal response of the COMARS assembly during Mars entry. The thermal model consists of a section of TPS and honeycomb structure with integrated COMARS sensor. The honeycomb/TPS structure is modeled as a solid structure with adjusted material properties (density, thermal conductivity, specific heat capacity). Some simplifications are made for the thermal model of the COMARS sensor. The honeycomb fixation screws, sensor housing, and D-Sub connector are neglected, as these parts are located at the back end of the sensor and do not influence the heat conduction from the TPS to the lower parts of the sensor. Furthermore the Pirani pressure sensor and the ICOTOM detectors are not incorporated in the thermal model as their thermal properties and inner layout are unknown. Because these parts are also located at the sensor back end, their influence on the thermal analysis is less significant. To evaluate the temperatures of pressure sensor and ICOTOM detectors, the temperature of the corresponding contact surface on the titanium holder is calculated. All contacts between the different parts are assumed to be in perfect thermal contact.

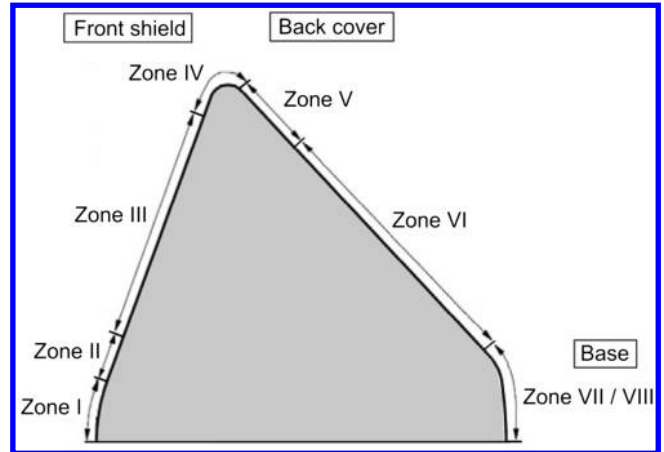


Fig. 8 Zone definition of the Schiaparelli capsule.

The Schiaparelli capsule is divided in different zones according to Fig. 8, which are defined by geometric and aerodynamic boundaries. There are overall eight different zones: stagnation region (zone I), sphere cone junction (zone II), midcone (zone III), shoulder region (zone IV), shoulder/rear cone junction (zone V), rear cone (zone VI), and base region (zones VII and VIII). The COMARS and broadband radiometer sensors are located on the back cover in zones V and VI. The heat flux used for the thermal simulation can be seen in Fig. 9 and is taken from the ExoMars EDM aerothermodynamic database [27].

The heat flux profiles in Fig. 9 represent the TPS sizing case and are the sum of convective and radiative heat flux. The convective heat flux was calculated for a wall temperature of 300 K and includes an uncertainty margin of 1.5–2 depending on the zone. The radiative heat flux part was considered to be conservative and does therefore not contain additional margins. The sudden drop in heat flux at $t = 175$ s results from a drop in the radiative heat flux component, which is not visible on the convective part. Unfortunately no explanation for the heat flux drop is given in the EDM aerothermodynamic database. The heat flux of zone VI is used for the thermal simulations because it is slightly higher than in zone V. The heat flux according to Fig. 9 is applied to the upper TPS surface, including the COMARS sensor surface. The simulation time is extended to 450 s to simulate further heat conduction into the material after the heat flux becomes zero (at $t = 250$ s). Radiation to ambient space with an emissivity of 0.9 is assumed for the TPS surface. All other outer surfaces are set to be adiabatic. A uniform starting temperature of 300 K is used for the simulation to be compliant with the wall temperature assumption used for the heat flux calculation. In Fig. 10 the temperature distribution inside the sensor is shown at the end of the simulation with a nearly homogeneous temperature of about 345 K. The resulting maximum temperatures of the different parts are presented in Fig. 11. The COMARS titanium holder reaches a maximum temperature of 400 K at the sensor front end (TPS side), whereas the contact surfaces for Pirani and ICOTOM sensors only

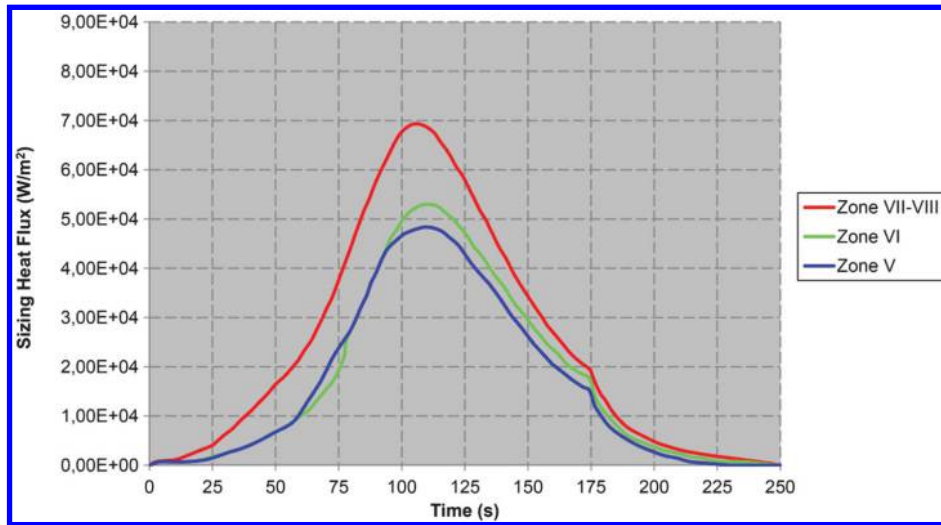


Fig. 9 Sizing heat flux profile for EDM back cover TPS [27].

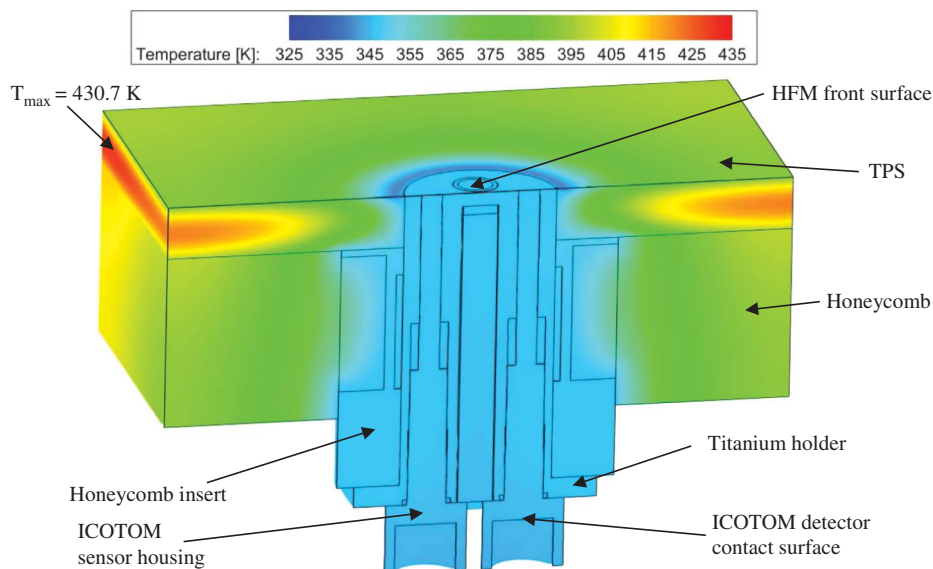


Fig. 10 Computed temperature distribution inside the COMARS sensor at the end of the simulation ($t = 450$ s).

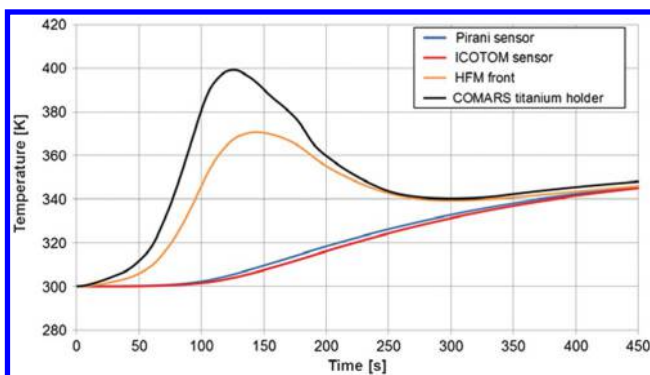


Fig. 11 COMARS sensor thermal simulation maximum temperatures.

heat up to a maximum of 345 K. All sensor parts are at a nearly homogeneous temperature level at the end of the simulation time.

The calculated temperatures of the COMARS sensor parts are summarized and compared with the corresponding maximum operative range in Table 2. The EDM back cover separation is assumed to take place at $t = 320$ s, which is the end of the sensor measurement. Therefore the maximum temperatures before this time point are used for comparison to the maximum operative

temperatures. All calculated values are inside the operative range, which ensures that the COMARS sensor can withstand the thermal environment during Mars entry. The actual temperature values during Mars entry will be lower than the temperatures shown in Table 2 because of the assumptions and simplifications used for the thermal analysis; for example,

- 1) The starting temperature will be much lower than the 300 K used in the simulation.
- 2) The assumption of perfectly bonded contacts between the different parts (perfect heat conduction) leads to higher sensor temperatures.
- 3) The used heat flux profile taken from the ExoMars EDM aerothermodynamic database represents the back cover TPS sizing case and therefore includes safety margins [27].

Table 2 Calculated temperatures compared with maximum operative temperatures for the different COMARS sensor parts

Part/contact surface	Maximum calculated temperature between $t = 0$ s and $t = 320$ s, K	Maximum operative temperature, K
Pirani pressure sensor	335	363
ICOTOM detector	332	348
Heat flux sensor	371	473
COMARS titanium holder	399	673

The temperature calculation represents a worst-case analysis considering the points listed above. Therefore no uncertainty analysis was conducted, for example, for uncertainties in material properties.

A simulation was performed only for the TPS structure using the same heat flux levels presented in Fig. 9 to verify that the implementation of the COMARS sensor will not lead to local overheating of TPS or honeycomb structure. A comparison of TPS and honeycomb structure temperatures with and without COMARS sensor showed that the maximum temperatures are lower for the case with a COMARS sensor due to a local heat sink effect (Fig. 12). Therefore the integration of the COMARS sensor into the TPS does not cause local overheating of TPS or honeycomb structure. The same is true for the broadband radiometer.

Another critical parameter is the temperature of the electronic box components during cruise. A transient thermal simulation was performed for the electronic box using conductive and radiative heat sink temperatures (thermal environment inside Schiaparelli) provided by TAS-I. A homogeneous starting temperature of 235 K and an adaptive time stepping with a maximum time step of 4000 s were used for the

simulation. The calculated minimum and maximum temperatures for the PCBs inside the electronic box (multiplexing and power board) are shown in Fig. 13. The identical maximum and minimum temperatures indicate that the box is in temperature equilibrium nearly the complete time. The only deviation that is visible occurs at the end of the calculation when the Mars entry takes place. At that time, in addition to the temperature rise due to Mars entry, the operating box dissipates energy. Because of this transient temperature environment the maximum and minimum temperatures are no longer identical.

Although an adaptive time stepping was used, the time step during the EDL phase is still comparably large. Therefore the temporal resolution of the entry phase is very low and the temperature rise during that phase only represents a rough calculation. But this is acceptable because the purpose of the simulation was to determine the electronic box temperatures during the cruise phase.

The presented results in Fig. 13 show that the box temperatures remain well above the minimum nonoperative/operative temperatures of 218 K. However, TAS-I installed a heater foil on the box casing to heat up the box in case it was needed.

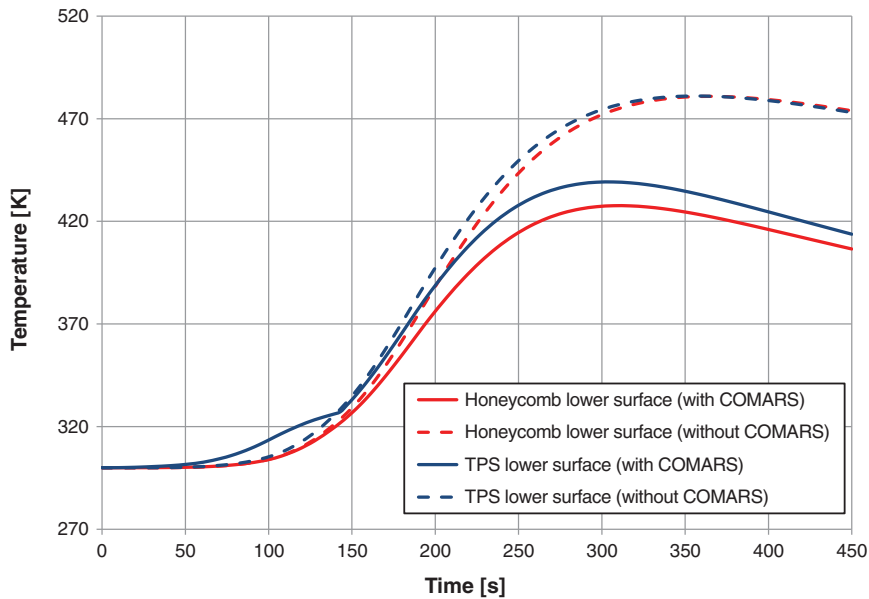


Fig. 12 TPS maximum temperatures with and without COMARS+ sensor.

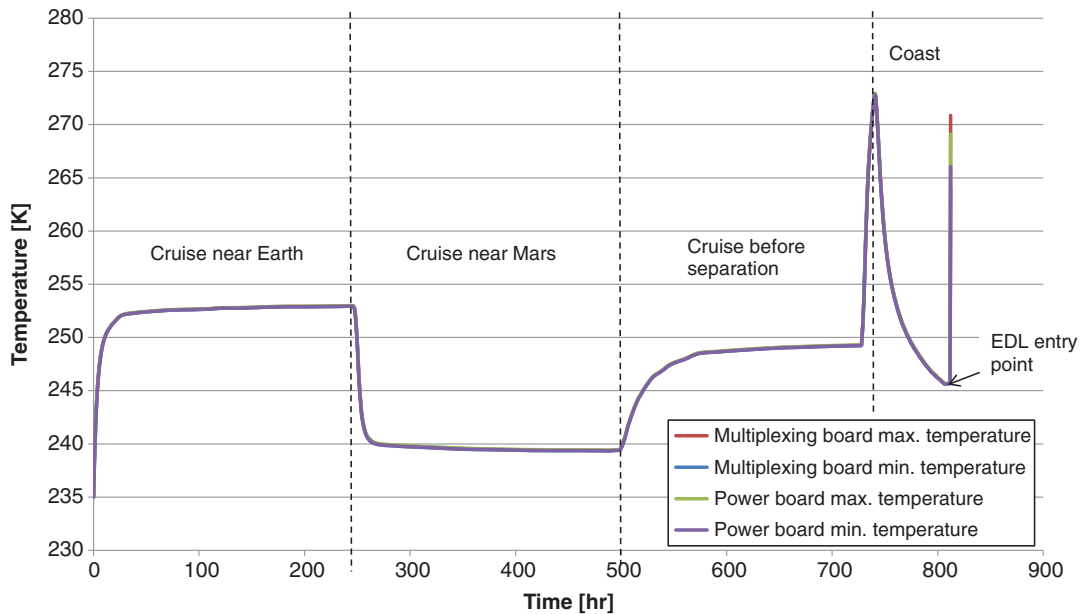


Fig. 13 Electronic box PCBs maximum and minimum temperatures during ExoMars flight.

Table 3 Parameters of aerothermal tests in L2K

Flow condition	Reservoir pressure, Pa	Total enthalpy, MJ/kg	Total temperature, K	CO ₂ mole fraction	Measured surface pressure, Pa	Measured surface total heat flux, kW/m ²
Low enthalpy	79,000	5.6	2815	0.546	225	25
High enthalpy	93,000	9.2	3283	0.227	270	45

V. Qualification and Acceptance Tests

The structural and thermal simulations described before were performed as worst-case analyses. No verification of the simulation results was performed by tests because the applied mechanical and thermal loads were conservative, in addition to the simplified boundary conditions that also represent conservative assumptions. Therefore the effect of inaccurate numerical modeling was neglected for these worst-case analyses. The design verification was done by extensive qualification and acceptance test campaigns. These tests included the following:

- 1) Vibration and shock tests to simulate all mechanical loads that occur during flight, like launch loads and stage separation shocks.
- 2) Thermal cycling tests under vacuum condition.
- 3) Electromagnetic compatibility (EMC) tests to check that the payload is compatible with the electromagnetic environment of the capsule and does not emit electromagnetic energy that could interfere with other devices.
- 4) Radiation tests for the COMARS+ sensors to verify radiation hardness.
- 5) Bioburden reduction and analyses to show the compliance with the planetary protection requirements.

A set of COMARS+ components was manufactured to perform qualification tests. These components had to pass all environmental tests listed above. Although the verification of the planetary protection requirements is not necessary for the qualification models, it was necessary to test the cleaning and bioburden reduction approach before applying it on the flight hardware. All qualification tests were performed successfully without any failures or malfunctions. Therefore no design updates were necessary between the qualification and flight models. The flight and spare models were qualified according to the acceptance test procedures incorporating mechanical, thermal/vacuum, and electromagnetic compatibility tests at acceptance level. After the final functional test and the verification of the planetary protection requirements, the payload components were packed in sterile bags and sent to TAS-I for integration into the Schiaparelli capsule.

All flight and flight spare model components and the necessary assembly tools were cleaned thoroughly with isopropanol before assembly using sterile wipes and an ultrasonic cleaner filled with isopropanol to satisfy the requirements concerning planetary protection. Cleaning and assembly were carried out in an ISO 5 laminar flow bench. Afterward all acceptance tests for the payload parts were conducted in an ISO 8 clean room environment. After successful completion of the tests, all accessible surfaces were again cleaned with isopropanol. In the final step all payload components except ICOTOM sensors, whose application temperature is limited to 75°C (348 K), were subjected to DHMR at 122°C (395 K) for 126 min (harness) and 166 min (other payload components). The temperature and time periods correspond to three orders of magnitude surface bioburden reduction for the harness cables and two orders of magnitude mated bioburden reduction for the payload components. After DHMR the payload components were brought to a ISO 1 clean room for a final functional check. The resulting bioburden of the COMARS+ payload was verified by several assays taken before the DHMR process and after the final functional test. Overall 22 samples were taken before DHMR and 9 samples after the functional test. All assays showed no colony forming units after 72 h of incubation, which satisfied the corresponding requirements for surface bioburden. Because the applied conditions for temperature and time during the DHMR process did not reduce the encapsulated bioburden of the COMARS+ hardware, the number of encapsulated spores was evaluated using bioburden level estimates for flight hardware according to the planetary protection

requirements document. The overall number of encapsulated spores, considering the complete volume of the nonmetallic payload components, amounts to 7096, which also satisfied the corresponding requirement.

Aerothermal tests were performed in the L2K facility of the Supersonic and Hypersonic Technology Department of DLR Cologne [28]. A representative wedge configuration with integrated qualification models was used for the final aerothermal tests [23]. This configuration is similar to the flight case because during Mars entry, the sensors are directly exposed to boundary-layer flow and radiation coming from the shock layer. The COMARS sensor and the broadband radiometer were integrated into the wind tunnel model at the same distance from the model holder nose tip to guarantee the same flow condition on both sensors. The tests were carried out at two different flow conditions because a complete duplication of the trajectory was not possible. While the high-enthalpy flow condition allowed achieving a total heat flux of 45 kW/m², which is quite close to the sizing heat flux of 50 kW/m², the measured total heat flux for the low-enthalpy flow condition was 25 kW/m². The parameters for the two flow conditions are summarized in Table 3.

A test run was conducted by starting with the low-enthalpy condition and then changing the parameters to the high-enthalpy condition. Afterward the flow condition was reset to the low-enthalpy case. The test showed a good repeatability of the pressure measurement within 4.5% of the measured pressure between the low-enthalpy test condition at the beginning and end of the test run. The deviation combines the measurement uncertainty of the pressure sensor ($\pm 5\%$ of the measured value) and the repeatability of the test condition itself. The corresponding total heat flux on the model surface showed a deviation of about 6% of the measured value between the beginning and end of the test run. The manufacturer of the heat flux sensor states a measurement uncertainty of $\pm 5\%$ (of the measured value) combining repeatability and calibration accuracy. But several wind-tunnel tests for which the same sensor was used and compared with different types of heat flux gauges indicate an increased uncertainty. Therefore, a maximum measurement uncertainty of $\pm 10\%$ is used as reference for the measured total heat fluxes.

The radiative heat flux is higher in the low-enthalpy case, which is linked to the higher concentration of carbon dioxide at lower enthalpy, which is the main contributor to the radiative heating. But even in the low-enthalpy case the measured radiative heat fluxes were in the order of a few kW/m². Because this is close to the lower measurement limit of the radiometer, no radiometer measurements are shown in the table. But the change in radiative heating, caused by the switching between the flow conditions, was clearly visible in the measured radiative heat flux [23].

VI. Flight Data

The main data package of the ExoMars EDL phase was stored on the lander, including the COMARS+ data as reported in [17,29]. Part of the flight data were transmitted to the TGO via telemetry at a low data rate. The data frequency of the transmitted COMARS+ data was 0.1 Hz. The main flight data should have been transmitted after successful landing. Unfortunately Schiaparelli's signal was lost about 43 s before the expected touchdown on Mars surface due to a malfunction during the final descent phase. Therefore ESA requested an independent inquiry, which identified an inconsistency between the inertial measurement unit (IMU) and radar Doppler altimeter (RDA) as reason for the failure [30]. The deployment and inflation of the parachute did cause lateral angular oscillations of the capsule above the saturation threshold of the IMU in one axis corrupting the estimated attitude because of its undo long persistence time. This led

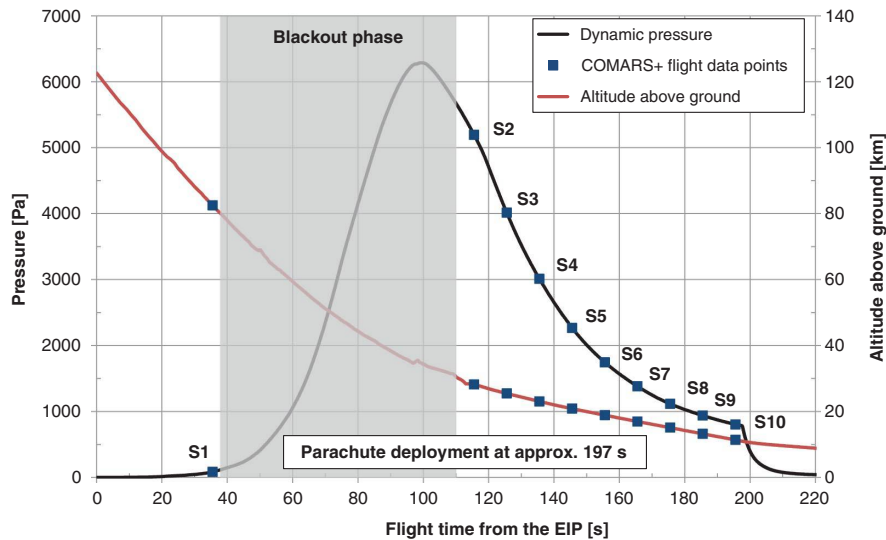


Fig. 14 Schiaparelli trajectory and COMARS+ data points.

to an inconsistency between IMU and RDA measurements, which resulted in wrong altitude calculation. Subsequent mode changes, conditioned on altitude, immediately triggered the back cover separation and activated the reaction control system (RCS) for the minimum time of 3 s, which ultimately led to the free fall of Schiaparelli from an altitude of around 3.7 km. Therefore COMARS+ flight data are only available with a sampling frequency of 0.1 Hz starting at the beginning of Mars entry and ending at parachute deployment but without the blackout phase.

The characteristics of the trajectory points at which COMARS+ data were transmitted, as estimated on the basis of level 0 postflight analyses, are given in Fig. 14 and Table 4 (values according to private communication with Stefano Portigliotti from TAS-I).

The first measurement point (S1) corresponds to 35 s after the entry interface point (EIP), which is defined as the flight time point with measurable deceleration (about 122 km altitude above ground). It will be shown later that the aerothermal heating on the back cover is negligible at times where the atmospheric density and thus dynamic pressure are low. The expected communication blackout phase approximately occurred between 37 and 106 s after EIP, so the next COMARS+ data point that was returned was at a time of 115 s (point S2). At this point the vehicle had decelerated to a velocity of 2595 m/s at an altitude of 28.2 km with a corresponding dynamic pressure and Mach number of 5193 Pa and 11.66, respectively. Atmospheric parameters are derived using an atmosphere model of the Mars climate database (MCD) version 4.3 from Laboratoire de Météorologie Dynamique (LMD), relying on atmosphere optical depth for the arrival date derived on the basis of NASA observations as well as trajectory reconstruction best estimates [31]. The last trajectory point (S10) is a few seconds ahead of the parachute deployment.

The measured housing temperatures of the COMARS pressure sensors were significantly lower than expected. Sensor structure temperatures between 273 and 323 K were assumed for the design of the instrumentation. But as shown in Fig. 15 the temperatures were around 245 K with a slight increase over the measurement time because of heat conduction from the sensor front end at the back cover surface. The temperature of COMARS3 was transmitted as part of the electronic box housekeeping data at lower sampling frequency because of limitations in the number of acquisition channels. Therefore COMARS3 housing temperature data were unfortunately not included in the reduced data package, which was transmitted during Mars entry via TGO. Because the temperature difference between COMARS1 and COMARS2 is small with a deviation of only 2.5 K, the temperature of COMARS 3 is expected to be within a few kelvins of the other two housing temperatures.

Because the calibration of the radiometer and pressure sensors depends also on the housing temperature, that is, detector temperature, COMARS+ spare sensors were re-calibrated after the flight at an extended temperature range from 243 to 323 K. This procedure also allowed checking the repeatability of the preflight calibration after the spare sensors were stored in sterilized bags for almost 2 years. The data reduction of all sensors was carried out using the relation between preflight and postflight calibration data.

The measured pressures at the three COMARS sensors are shown in Fig. 16. All three sensors, which have a measurement uncertainty of $\pm 5\%$ (of the measured value), measured almost the same pressure level. This behavior with almost no spatial gradient can be explained by separated flow on the back cover of the capsule due to flow separation at the vehicle shoulder. The pressure of COMARS3 at trajectory point S2 is 146 Pa and the predicted dynamic pressure is

Table 4 Trajectory points with available COMARS+ flight data

	Flight time from EIP, s	Altitude above ground, km	Speed, m/s	Atmospheric density, kg/m^3	Atmospheric pressure, Pa	Atmospheric temperature, K	Mach number	Dynamic pressure, Pa
EIP	0	122.6	6001.39	$3.306\text{E} - 08$	0.0008	126.27	32.320	0.595
S1	35.553	82.467	5829.38	$5.092\text{E} - 06$	0.16	165.50	27.946	86.53
Communication blackout								
S2	115.553	28.202	2595.41	$1.542\text{E} - 03$	56.56	191.58	11.665	5193.40
S3	125.551	25.477	2013.84	$1.979\text{E} - 03$	74.13	195.38	8.967	4013.02
S4	135.552	23.064	1570.58	$2.440\text{E} - 03$	93.15	199.13	6.935	3009.56
S5	145.551	20.862	1236.92	$2.962\text{E} - 03$	114.57	202.28	5.431	2265.92
S6	155.551	18.887	1001.92	$3.478\text{E} - 03$	137.21	205.79	4.360	1745.64
S7	165.553	16.959	823.09	$4.078\text{E} - 03$	163.84	209.69	3.553	1381.21
S8	175.551	15.099	685.40	$4.751\text{E} - 03$	194.15	213.67	2.937	1115.89
S9	185.552	13.227	584.38	$5.496\text{E} - 03$	228.85	217.40	2.483	938.40
S10	195.551	11.379	503.09	$6.355\text{E} - 03$	269.55	221.63	2.120	804.24

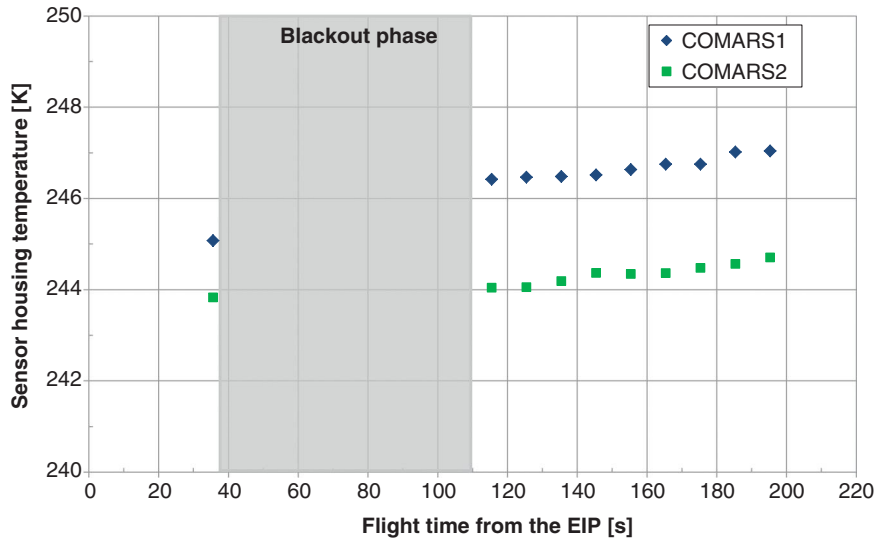


Fig. 15 Measured sensor housing temperatures of COMARS1 and COMARS2 sensors during Schiaparelli entry flight.

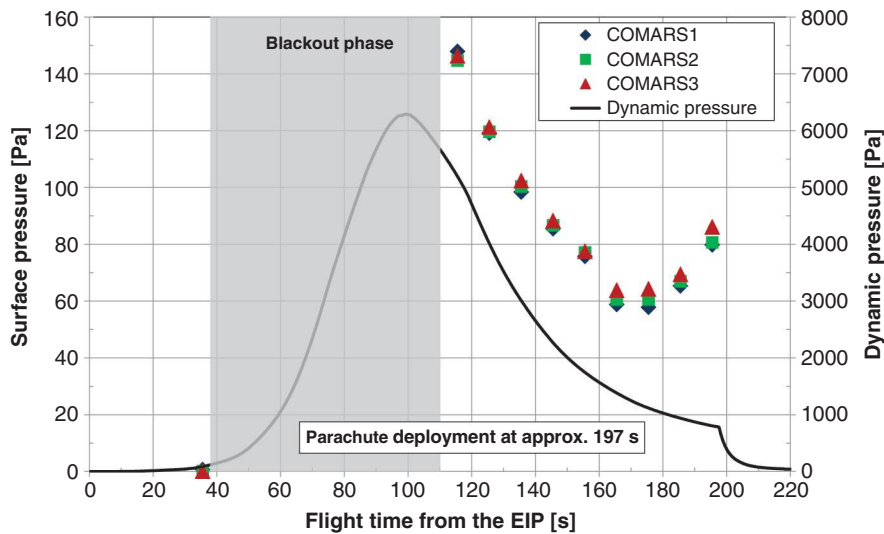


Fig. 16 Measured back cover surface pressure during Schiaparelli entry flight.

5193 Pa. The corresponding pressure coefficient c_p , which is defined as the difference between measured pressure and free stream atmospheric pressure divided by dynamic pressure [see Eq. (1)], is 0.0172. The pressure coefficient at the front cover stagnation point, evaluated using preliminary computations [31], is calculated as 1.929. This means that the surface pressure close to the shoulder on the back cover is approximately 0.9% of the front cover stagnation point pressure.

$$c_p = \frac{p_{\text{measured}} - p_{\infty}}{q_{\infty}} \quad (1)$$

If we consider that the peak value of back cover in-depth temperatures occurs significantly later than the blackout phase [17], measured pressure data should not be far from the peak pressure on the back cover. Until a flight time point of 170 s from the EIP the decreasing surface pressure corresponds well to the dynamic pressure evolution (see Table 4). After this point an increase of the surface pressure is observed. One explanation for this behavior could be a change of the flow regime in the wake. From earlier studies it is known that depending on Reynolds number and front surface roughness, the wake flow may change from laminar to turbulent regime [32]. This leads to a shorter wake, which influences

the dynamic stability and can cause an increase of the base pressure. Unfortunately there was no base pressure measurement (zone VII/VIII in Fig. 8) to confirm this assumption. There are also no CFD calculations available to determine the surface pressure difference between laminar and turbulent wake flow. In any case a CFD simulation of the wake flow is difficult due to flow separation, an unsteady vortical flow field, and embedded rarefied flow in the capsule wake leading to inaccurate computation results.

Another reason for the pressure increase after the flight time point of 170 s could be a change in the total angle of attack that influences the wake flow field. The total angle of attack, evaluated from preliminary FADS reconstruction, shows an increase from about 1 deg at 146 s to about 10 deg at 195 s [33]. The effect of an increasing total angle of attack on the back cover surface pressure in a separated and instationary flow field is difficult to predict and requires further CFD analyses or wind tunnel tests.

Corresponding pressure coefficient values measured with COMARS3, COMARS2, and COMARS1 sensors at trajectory points S2, S3, and S4 are listed in Table 5.

The total heat flux rate was measured directly by the heat flux microsensor incorporated into the COMARS sensor design (Fig. 2). The COMARS3 sensor, located close to the back cover shoulder, measured significantly higher heat fluxes compared with sensors

Table 5 Pressure coefficients at the locations of the COMARS sensors at trajectory points S2, S3, and S4

Trajectory point	Pressure coefficient c_p		
	COMARS3	COMARS2	COMARS1
S2	0.0172	0.0170	0.0176
S3	0.0117	0.0112	0.0129
S4	0.0029	0.0023	0.0016

COMARS1 and COMARS2 (see Figs. 1 and 17). It is interesting to see that at trajectory point S3 COMARS1 measures a higher value than COMARS2. At this moment there is no explanation for the heat flux trends, but it has to be mentioned that the base flow is highly unsteady. In addition, the heat flux measurement uncertainty ($\pm 10\%$ of the measured value) has to be taken into account.

The main driving factors for the measurement accuracy at low heat fluxes are the signal-to-noise ratio and the accurate determination of the sensor output voltage. During the COMARS sensor calibration a black body source was used with heat flux values down to about 2 kW/m^2 , but no assessment for the measurability of smaller heat fluxes was performed. Therefore the heat fluxes at the trajectory points S1 and S5–S10 (with levels below 2 kW/m^2) are considered too low for a credible assessment.

An evaluation of the Stanton number defined in Eq. (2) has been performed to show the relation between measured heat fluxes on the back cover and the total energy of the gas in the shock layer. In this equation the recovery factor is set to one and the wall temperature is assumed to be 300 K. Because the heat flux sensor is made out of metal material with a high thermal conductivity and measured structure temperatures are around 245 K (see Fig. 15), this assumption is justified. The Stanton numbers for the COMARS sensors are evaluated using the measured total heat flux and the free stream atmospheric parameters according to Table 4. The use of local boundary-layer edge parameters may be more suitable, but this requires dedicated CFD computations, including the simulation of a partially separated wake flow.

$$St = \frac{\dot{q}_{\text{meas}}}{\rho_{\infty} u_{\infty} (h_0 - h_w)} \quad (2)$$

The calculated Stanton numbers for the COMARS sensors at S2, S3, and S4 are shown in Table 6 together with the front cover stagnation point Stanton numbers. The Stanton numbers for COMARS3 are approximately one order of magnitude lower than the front cover stagnation point Stanton numbers.

The front cover stagnation point heat flux is calculated according to Sutton–Graves formula [Eq. (3)] [34] for spherical bodies assuming

Table 6 Stanton number values at trajectory points S2, S3, and S4

Trajectory point	Stanton number St			
	COMARS3	COMARS2	COMARS1	Front cover stagnation point
S2	0.00116	0.00089	0.00089	0.01323
S3	0.00075	0.00045	0.00059	0.01186
S4	0.00065	0.00051	0.00033	0.01096

Table 7 Ratio of measured back cover total heat fluxes to calculated front cover stagnation point heat fluxes

Trajectory point	$\dot{q}_{\text{meas}}/\dot{q}_s$		
	COMARS3	COMARS2	COMARS1
S2	0.09	0.07	0.07
S3	0.06	0.04	0.05
S4	0.06	0.05	0.03

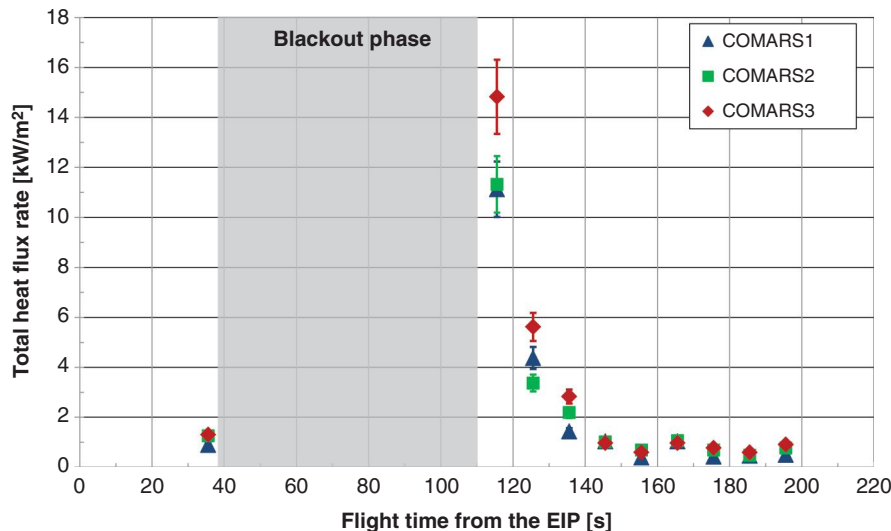
cold-wall boundary conditions. In addition to free stream atmospheric density and vehicle velocity, further necessary parameters are the constant k , which is set to $1.9027 \times 10^{-4} \sqrt{\text{kg/m}}$ for Mars atmosphere [34] and the nose radius R_n .

$$\dot{q}_s = k \left(\frac{\rho_{\infty}}{R_n} \right)^{1/2} u_{\infty}^3 \quad (3)$$

Because the Schiaparelli capsule is not a spherical body, an equivalent nose radius has to be used, which depends on capsule geometry, atmospheric parameters, and velocity. In this case the equivalent nose radius is just set to the nose radius of the Schiaparelli capsule (0.6 m), which is a conservative assumption.

The highest ratio of the heat flux rate measured with COMARS3 to the predicted front cover stagnation point heat flux rate is approximately 0.09 at trajectory point S2. This ratio decreases to approximately 0.06 for trajectory points S3 and S4, respectively. In case of sensors COMARS2 and COMARS1, which are located farther away from the vehicle shoulder, the ratios are approximately 0.07 at trajectory point S2 and 0.03 to 0.05 at trajectory points S3 and S4. Table 7 lists the calculated ratios for the different trajectory points. These ratios can be used to estimate aerothermal loads on the back cover using calculated front cover stagnation point heat fluxes from CFD or simplified methods like Sutton–Graves [Eq. (3)].

Figure 18 shows a comparison between the total heat flux rate of COMARS3 and the radiative heat flux rate measured with the broadband radiometer, which are located close to each other (Fig. 1). At trajectory point S2 the measured radiative heat flux is

**Fig. 17** Measured total heat flux rate on the back cover during Schiaparelli entry flight including error bars.

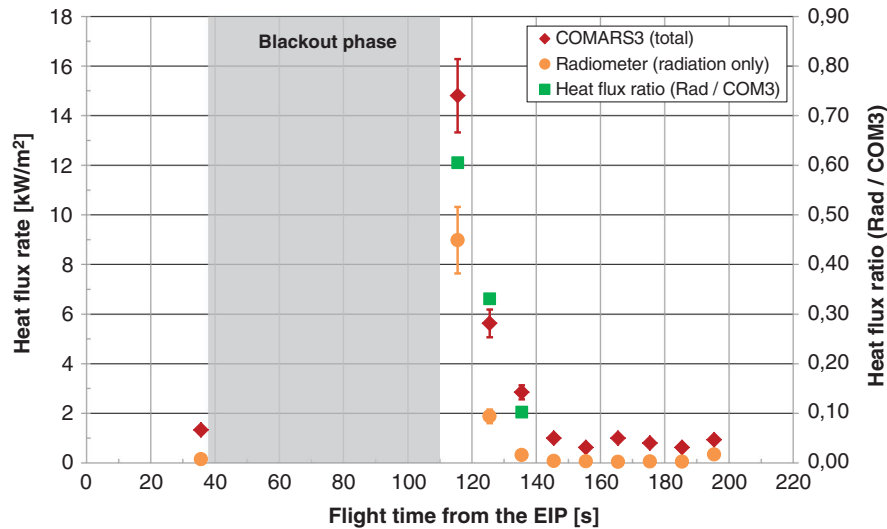


Fig. 18 Measured total heat flux, radiative heat flux, and ratio of radiative to total heat flux on the back cover during Schiaparelli entry flight including error bars.

9.0 kW/m². The corresponding ratio of radiative heat flux rate to total heat flux rate for trajectory point S2 is therefore 0.61. This ratio decreases to 0.33 for trajectory point S3 and 0.1 for trajectory point S4. The measured heat fluxes at trajectory points S1 and S5–S10 are too low for a qualified assessment. Figure 18 also includes error bars for the radiometer measurements. The measurement uncertainty determined during calibration is $\pm 15\%$ of the measured value. The calibration was performed using a large area black body source (200 × 200 mm). By placing the radiometer very close to the black body surface the only radiation entering the conical borehole of the radiometer is emitted by the isothermal black body surface. The calibration curve was created by applying different black body temperatures. Therefore no view angle correction was necessary despite the conical borehole.

The high contribution of radiative heating (61%) to the overall aerothermal heating close to the shoulder region at trajectory point S2 is an important result of the broadband radiometer measurement. The ratio decreases with increasing distance from the shoulder [25]. This result is important for the design of back cover TPS because it means that Mars entry aerothermal analysis should include an estimate for shock layer radiation. But it has to be mentioned that measured back cover heat fluxes for Schiaparelli are far below the sizing total heat flux level of approximately 50 kW/m² (Fig. 9) [27]. Because the peak heating on front and back cover occurred during the communication blackout, where no flight data is available, the hypothesis that the back cover heating maximum is delayed with respect to the front cover peak heating (as mentioned in Ref. [5]) cannot be confirmed.

The postflight analysis of the narrow band radiometers (ICOTOM sensors), contributed by the French space agency CNES (see Sec. III), is in progress.

VII. Conclusions

The instrumentation package COMARS+ consisted of three combined aerothermal sensors, one broadband radiometer sensor, and an electronic box and was flown at three locations on the back cover of the ExoMars Schiaparelli capsule. The aerothermal sensors called COMARS combined four discrete sensors, measuring static pressure, total heat flux, temperature, and radiative heat flux, at two specific spectral bands. The infrared radiation in a broadband spectral range was measured by the separate broadband radiometer sensor. The electronic box of the payload was used for amplification, conditioning, and multiplexing of the sensor signals. The design ended with a total mass of 1.73 kg and a power consumption of 4.5 W for the complete payload.

Although the landing of Schiaparelli failed, part of the flight data during the entry phase were transmitted to the orbiter at a low sampling rate. All COMARS+ sensors delivered useful data with respect to total heat flux rate, radiative heat flux rate, surface temperature, and surface pressure from the atmospheric entry point until parachute deployment with the exception of the plasma blackout phase. Because measured structure and sensor housing temperatures were below predicted preflight values, a further calibration using the COMARS+ spare sensors at temperatures down to 243 K was conducted. The main results of the COMARS+ in-flight measurements can be summarized as follows:

1) The radiative heat flux on the back cover near the vehicle shoulder was measured successfully. At the first trajectory point after communication blackout the measured radiative heat flux is 9.0 kW/m², or 61% of the total heat flux. This value decreases to 33% for the trajectory point 10 s later. These results confirm an important radiative contribution to the total heating on the back cover.

2) The highest ratio of the measured total heat flux rate to the calculated front cover stagnation point heat flux rate occurred close to the vehicle shoulder (COMARS3) immediately after the communication blackout with a value of approximately 0.09. This ratio decreases to approximately 0.06 for later trajectory points. At the sensors COMARS2 and COMARS1, which are located at larger distances from the vehicle shoulder, the ratio directly after communication blackout is approximately 0.07 and decreases to roughly 0.05–0.03 later in the trajectory.

3) Pressure measured at three back cover locations showed almost no dependency on measurement location, as the pressures were very similar in magnitude and temporal behavior. This finding is believed to be the result of separated aftbody flowfield at the measurement locations. An unexpected pressure increase was measured late in the entry trajectory after peak dynamic pressure. Possible explanations for this behavior could be a change of the wake flow from laminar to turbulent regime or a variation in angle of attack that influences the wake flow field.

4) Measured back cover total heat fluxes are below the sizing total heat flux level of the back cover TPS. This very important result suggests that the design margins of the back cover TPS design can be reduced.

Further flight data analyses should be performed using CFD calculations for the back cover region. A dedicated computational flowfield analysis is recommended to further investigate the observed pressure increase late in the trajectory about 170 s after the EIP. Although back cover heat flux data are only available at a few trajectory points, the measured radiative and total heat flux directly after the communication blackout can be used for comparison with calculated values from CFD analyses performed using the

reconstructed trajectory parameters. This is important because the prediction of aerothermal loads on the back cover, using existing experimental and numerical tools, is very complex and still has large uncertainties especially concerning radiative heating.

Acknowledgments

The authors wish to thank Olivier Bayle (ESA) for his significant and continuous support for the implementation of the COMARS+ on-board Schiaparelli and for the decision to transmit a subset of COMARS+ data during the entry phase, and Stefano Portigliotti (TAS-I) for all fruitful technical discussions and his support during the post-flight analysis.

References

- [1] Beck, J., Tran, Ph., and Walpot, L., "Aerothermodynamics of the ExoMars Entry Demonstrator Module," *Proceedings of 7th European Symposium on Aerothermodynamics*, ESA Communications Paper ESA SP-692, The Netherlands, Aug. 2011.
- [2] Beck, J., Omaly, P., Lino da Silva, M., and Surzhikov, S., "Radiative Heating of the ExoMars Entry Demonstrator Module," *Proceedings of 7th European Symposium on Aerothermodynamics*, ESA Communications Paper ESA SP-692, The Netherlands, Aug. 2011.
- [3] Lino da Silva, M., and Beck, J., "Contribution of CO₂ IR Radiation to Martian Entries Radiative Wall Fluxes," *49th AIAA Aerospace Sciences Meeting Including the New Horizons Forum and Aerospace Exposition*, AIAA, Reston, VA, Aug. 2011, <https://arc.aiaa.org/doi/10.2514/6.2011-135>.
- [4] Ingoldby, R. N., Michel, F. C., Flaherty, T. M., Doryand, M. G., Preston, B., Villyard, K. W., and Steele, R. D., "Entry Data Analysis for Viking Landers 1 and 2 Final Report," NASA CR-159388, Nov. 1976.
- [5] Edquist, K. T., Wright, M. J., and Allen, G., "Viking Afterbody Heating Computations and Comparisons to Flight Data," *44th AIAA Aerospace Sciences Meeting and Exhibit*, AIAA Paper 2006-386, Jan. 2006, <https://arc.aiaa.org/doi/10.2514/6.2006-386>.
- [6] Milos, F. S., "Galileo Probe Heat Shield Ablation Experiment," *Journal of Spacecraft and Rockets*, Vol. 34, No. 6, 1997, pp. 705–713. doi:10.2514/2.3293
- [7] Milos, F. S., Chen, Y.-K., Congdon, W. M., and Thornton, J. M., "Mars Pathfinder Entry Temperature Data, Aerothermal Heating, and Heatshield Material Response," *Journal of Spacecraft and Rockets*, Vol. 36, No. 3, 1999, pp. 380–391. doi:10.2514/2.3457
- [8] Edquist, K. T., Dyakonov, A. A., Wright, M. J., and Tang, C. Y., "Aerothermodynamic Design of the Mars Science Laboratory Heatshield," *41st AIAA Thermophysics Conference*, AIAA Paper 2009-4075, 2009. doi:10.2514/6.2009-4075
- [9] Wright, M. J., Beck, R. A. S., Edquist, K. T., Driver, D., Sepka, S. A., Slimko, E. M., Wilcockson, W. H., DeCaro, A., and Hwang, H. H., "Sizing and Margins Assessment of the Mars Science Laboratory Aeroshell Thermal Protection System," AIAA Paper 2009-4231, June 2009. doi:10.2514/6.2009-4231
- [10] Little, A., Bose, D., Karlgaard, C., Munk, M., Kuhl, C., Schoenenberger, M., Antill, C., Verhappen, R., Kutty, P., and White, T., "The Mars Science Laboratory (MSL) Entry, Descent and Landing Instrumentation (MEDLI): Hardware Performance and Data Reconstruction," *36th AAS Guidance and Control Conference*, Breckenridge, CO, Feb. 2013.
- [11] Bose, D., White, T., Santos, J. A., Feldman, J., Mahzari, M., Olson, M., and Laub, B., "Initial Assessment of Mars Science Laboratory Heatshield Instrumentation and Flight Data," AIAA Paper 2013-0908, Jan. 2013. doi:10.2514/6.2013-908
- [12] Bose, D., White, T., Mahzari, M., and Edquist, K. T., "Reconstruction of Aerothermal Environment and Heat Shield Response of Mars Science Laboratory," *Journal of Spacecraft and Rockets*, Vol. 51, No. 4, 2014, pp. 1174–1184. doi:10.2514/1.A32783
- [13] Karlgaard, C. D., Kutty, P., Schoenenberger, M., Shidner, J., and Munk, M., "Mars Entry Atmospheric Data System Trajectory Reconstruction Algorithms and Flight Results," AIAA Paper 2013-0028, Jan. 2013. doi:10.2514/6.2013-28
- [14] Schoenenberger, M., Norman, J. V., Karlgaard, C., Kutty, P., and Way, D., "Assessment of the Reconstructed Aerodynamics of the Mars Science Laboratory Entry Vehicle," *Journal of Spacecraft and Rockets*, Vol. 51, No. 4, 2014, pp. 1076–1093. doi:10.2514/1.A32794
- [15] Bayle, O., Lorenzoni, L. V., Blancquaert, T., Langlois, S., Walloschek, T., Portigliotti, S., and Capuano, M., "ExoMars Entry Descent and Landing Demonstrator Mission and Design Overview," *8th International Planetary Probe Workshop*, Portsmouth, VA, June 2011, <https://pub-lib.jpl.nasa.gov/docushare/dsweb/View/Collection-1141>.
- [16] Lorenzoni, L. V., "ExoMars 2016 Entry Descent and Landing Overview," *10th International Planetary Probe Workshop*, San Jose, CA, June 2013, <https://pub-lib.jpl.nasa.gov/docushare/dsweb/View/Collection-1139>.
- [17] Portigliotti, S., Cassi, C., Montagna, M., Martella, P., Faletta, M., Boi, J., De Sanctis, S., Granà, D., Bayle, O., Blancquaert, T., and Lorenzoni, L., "ExoMars 2016, the Schiaparelli Mission. EDL Demonstration Results from Real Time Telemetry Before Unfortunate Impact," *14th International Planetary Probe Workshop*, The Hague, The Netherlands, June 2017, <https://pub-lib.jpl.nasa.gov/docushare/dsweb/View/Collection-1152>.
- [18] Wright, M. J., Milos, F. S., and Tran, P., "Afterbody Aeroheating Flight Data for Planetary Probe Thermal Protection System Design," *Journal of Spacecraft and Rockets*, Vol. 43, No. 5, 2006, pp. 929–943. doi:10.2514/1.17703
- [19] Brandis, A. M., Saunders, D. A., Johnston, C. O., Cruden, B. A., and White, T. R., "Radiative Heating on the After-Body of Martian Entry Vehicles," *45th AIAA Thermophysics Conference*, AIAA Paper 2015-3111, June 2015. doi:10.2514/6.2015-3111
- [20] Eggers, T., Longo, J., Turner, J., Jung, W., Hörschgen, M., Stamminger, M., Gülhan, A., Siebe, F., Requardt, G., Laux, T., Reimer, T., and Weihs, H., "The SHEFEX Flight Experiment—Pathfinder Experiment for a Sky Based Test Facility," *14th AIAA/AHI Space Planes and Hypersonic Systems and Technologies Conference*, AIAA Paper 2006-7921, Nov. 2006. doi:10.2514/6.2006-7921
- [21] Gülhan, A., Siebe, F., Thiele, T., Neeb, D., Turner, J., and Ettl, J., "Sharp Edge Flight Experiment-II Instrumentation Challenges and Selected Flight Data," *Journal of Spacecraft and Rockets*, Vol. 51, No. 1, 2014, pp. 175–186. doi:10.2514/1.A32572
- [22] Gülhan, A., Thiele, T., and Siebe, F., "Combined Sensor Assembly COMARS+ for ExoMars EDM Demonstrator," *7th European Workshop on Thermal Protection Systems and Hot Structures*, ESA Publ. Div., The Netherlands, 2013.
- [23] Gülhan, A., Thiele, T., Siebe, F., and Kronen, R., "Combined Instrumentation Package COMARS+ for the ExoMars Schiaparelli Lander," *Space Science Reviews*, Vol. 214, Feb. 2018, p. 12. doi:10.1007/s11214-017-0447-4
- [24] Omaly, P., and Hebert, P. J., "ICOTOM: Integrated Narrow Band Infrared Radiometer," *11th International Planetary Probe Workshop*, Pasadena, CA, June 2014, <https://pub-lib.jpl.nasa.gov/docushare/dsweb/View/Collection-1138>.
- [25] Gülhan, A., Thiele, T., Siebe, F., Schleutker, T., Kronen, R., Annaloro, J., Omaly, P., and Hebert, P. J., "Achievements of the COMARS+ Instrumentation Package During the Entry Flight Phase of the ExoMars Schiaparelli Lander," *14th International Planetary Probe Workshop*, The Hague, The Netherlands, June 2017, <https://pub-lib.jpl.nasa.gov/docushare/dsweb/View/Collection-1152>.
- [26] Miles, J. W., "On Structural Fatigue under Random Loading," *Journal of the Aeronautical Sciences*, Vol. 21, No. 11, 1954, pp. 753–762. doi:10.2514/8.3199
- [27] Venditto, P., "ExoMars EDM Aerothermodynamic Database (ATDB)," Thales Alenia Space, Internal Document, EXM-DM-TNO-AI-0059, Controlled Distribution, Issue 7, July 2011.
- [28] Gülhan, A., and Esser, B., "Arc-Heated Facilities as a Tool to Study Aerothermodynamic Problems of Re-Entry Vehicles," *Advanced Hypersonic Test Facilities*, edited by F. K. Lu, and D. E. Marren, Progress in Astronautics, and Aeronautics, Vol. 198, AIAA, Reston, VA, 2002, pp. 375–403, <https://arc.aiaa.org/doi/10.2514/5.9781600866678.0375.0403>.
- [29] Blancquaert, T., Bayle, O., Lorenzoni, L. V., and Ball, A. J., "ExoMars Entry, Descent and Landing Demonstrator Schiaparelli: Flight Overview and Mission Results," *14th International Planetary Probe Workshop*, The Hague, The Netherlands, June 2017, <https://pub-lib.jpl.nasa.gov/docushare/dsweb/View/Collection-1152>.
- [30] Tolker-Nielsen, T., "ExoMars 2016 Schiaparelli Anomaly Inquiry," Issue 1, May 2017, <http://exploration.esa.int/mars/59176-exomars-2016-schiaparelli-anomaly-inquiry/>.
- [31] Bonetti, D., De Zaiacomo, G., Blanco, G., Pontijas Fuentes, I., Portigliotti, S., Bayle, O., and Lorenzoni, L., "ExoMars 2016: Schiaparelli Coasting, Entry and Descent Post Flight Mission Analysis,"

- 68th International Astronautical Congress (IAC)*, Adelaide, Australia, Sept. 2017, <https://iafaastro.directory/iac/archive/browse/IAC-17/>.
- [32] Gülhan, A., Klevanski, J., and Willems, S., "Experimental Study of the Dynamic Stability of the ExoMars Capsule," *Proceedings of 7th European Symposium on Aerothermodynamics*, ESA Communications Paper ESA SP-692, The Netherlands, Aug. 2011.
- [33] Van Hove, B., Karatekin, Ö., Schleutker, T., and Gülhan, A., "Surface Pressure Data from ExoMars Schiaparelli Instrumented Heat Shield," *14th International Planetary Probe Workshop*, The Hague, The Netherlands, June 2017, <https://pub-lib.jpl.nasa.gov/docushare/dsweb/View/Collection-1152>.
- [34] Dec, J. A., and Braun, R. D., "An Approximate Ablative Thermal Protection System Sizing Tool for Entry System Design," *44th AIAA Aerospace Sciences Meeting and Exhibit*, AIAA Paper 2006-780, Jan. 2006, <https://arc.aiaa.org/doi/10.2514/6.2006-780>.

K. T. Edquist
Associate Editor